THE JOURNAL OF PHYSICAL CHEMISTRY C

pubs.acs.org/JPCC Article

Intermediate Species in the Crystallization of Sodium Aluminate Hydroxy Hydrates

Trent R. Graham,* Mateusz Dembowski, Jian Zhi Hu, Nicholas R. Jaegers, Xin Zhang, Sue B. Clark, Carolyn I. Pearce, and Kevin M. Rosso*

Cite This: J. Phys. Chem. C 2020, 124, 12337−12345 Read Online

ACCESS | Metrics & More | Article Recommendations | Supporting Information

ABSTRACT: In highly alkaline "water-in-salt" $Na_2O/Al_2O_3/H_2O$ solutions where the monomeric $Al(OH)_4^-$ anion dominates, isolation of transitional species that seed crystallization of sodium aluminate salt hydrates has been challenging. For example, discrimination of dimeric [for example, $Al_2O(OH)_6^{2-}$] species via ^{27}Al nuclear magnetic resonance (NMR) spectroscopy is limited via fast interconversion through hydrolysis and condensation reactions. Despite this, using magic-angle spinning NMR (^{27}Al MAS NMR) at high magnetic field strengths (14.1 and 20.0 T) on crystals of nonasodium bis(hexahydroxyaluminate) trihydroxide hexahydrate [NSA, $Na_9[Al(OH)_6]_2{\cdot}3(OH){\cdot}6(H_2O)$], we observed a ^{27}Al resonance consistent with $Na_2Al_2O(OH)_6$. This tetrahedral dimeric species was also identified in the mother liquor by Raman spectroscopy while remaining expectedly unresolved by high-field liquid-state ^{27}Al NMR. Its substantial abundance in the mother liquor and as either an interstitial or an adsorbate on precipitated solids suggest that it plays a crucial role in NSA crystallization. Our detailed characterization, which includes single-pulse ^{27}Al MAS NMR, nutation ^{27}Al MAS NMR, and multiple quantum ^{27}Al MAS NMR, provides new molecular insights into how aluminate transitions from tetrahedral in solution to octahedral in solid. This understanding could ultimately lead to better predictions of aluminum phase change behavior in caustic sodium hydroxide with wide-ranging technological and environmental implications.

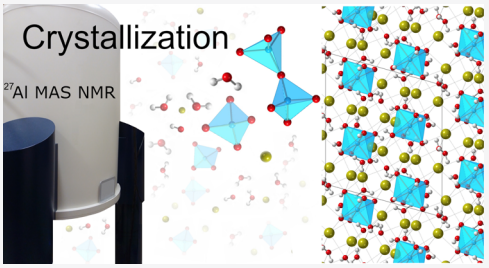

1. INTRODUCTION

The dominant form of aluminum (Al^{3+}) in highly alkaline "water-in-salt" solutions of sodium, potassium, cesium, tetramethylammonium, and rubidium hydroxide is the monomeric tetrahedral aluminate anion ($Al(OH)_4^-$), whereas in coexisting solids, Al^{3+} is typically of higher coordination number and/or polymerization extent.[1,2] Processes such as precipitation and dissolution therefore entail a relatively rapid coordination change of Al^{3+} on the molecular scale. Structure regulation at interfaces may play an important role in facilitating this coordination change[3,4] as well as ion pairing interactions because of the limited availability of waters of hydration.[5,6] Capturing transitional Al^{3+} species is thus of interest for understanding the mechanism of crystallization and the role of distinct cations.

One potentially important species is the μ-oxo aluminate dimer ($Al_2O(OH)_6^{2-}$), which can form by oxolation in solution and, in concentrated potassium and rubidium hydroxide, leads directly to crystallization of $M_2Al_2O(OH)_6$ salts (M = K^+ or Rb^+), principally comprised of this dimer motif.[1,2,7−9] However, crucially, in the sodium system, no comparable sodium aluminate dimer crystal structure has been found despite thorough exploration of the $Na_2O/Al_2O_3/H_2O$ phase diagram.[10−17] Analysis of the formation, reactivity, and dynamics of $Al_2O(OH)_6^{2-}$ in solution is challenging because of rapid exchange of Al^{3+} ion speciation through hydrolysis and condensation during nuclear magnetic resonance (NMR) spectroscopy,[1,2,6,18,19] degenerate Raman-active vibrational modes,[20] nonmonotonic trends in pre-edge features in X-ray absorption spectroscopy,[21] and multimodal relaxation processes in both dielectric spectroscopy[22] and quasielastic neutron scattering.[18] Among such techniques, the most diagnostic is Raman spectroscopy, which clearly shows that vibrational modes of sodium aluminate solutions contain a component similar to that of $K_2Al_2O(OH)_6$.[8,23,24]

Because Al^{3+} speciation is often manipulated in highly concentrated sodium hydroxide solutions, such unresolved questions have impeded a mechanistic understanding of rate-limiting steps during nucleation, precipitation, and dissolution.[25] For example, in addition to aspects of aluminum refining[26] and corrosion sciences,[27] this knowledge gap impacts the processing of radioactive high-level waste (HLW), currently stored in underground tanks at the U.S. Department of Energy sites such as the Hanford Nuclear Reservation, Washington.[28,29] These wastes are highly caustic,

Received: January 8, 2020
Revised: March 14, 2020
Published: April 15, 2020

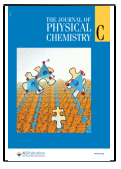

https://dx.doi.org/10.1021/acs.jpcc.0c00205
J. Phys. Chem. C 2020, 124, 12337−12345

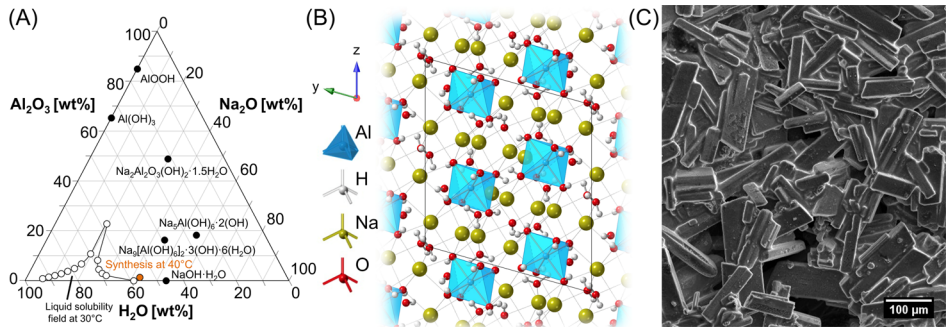

Figure 1. (A) Ternary phase diagram of $Na_2O/Al_2O_3/H_2O$ system. Relevant phases are denoted in black. The solubility field at 30 °C is bound by measurements denoted in white.[58,59] The synthesis initial composition, 31.3 m NaOH and 0.6 m Al^{3+}, is denoted in orange. The synthesis utilizes slow evaporation to initiate precipitation of NSA. The ternary diagram was illustrated in Triplot (v. 1.4).[60] (B) Crystal structure of NSA, $Na_9[Al(OH)_6]_2 \cdot 3(OH) \cdot 6(H_2O)$. (C) Scanning electron micrograph of the NSA crystals.

with hydroxide concentrations typically over 1 M and sodium concentrations reaching 11 M on average.[28,29] The waste is rich in Al^{3+}, introduced as an ionic strength buffer during ion separations by codisposal and leaching of Al^{3+} from fuel cladding and by addition of aluminum nitrate to reduce corrosion.[28] Coexisting Al^{3+} solids occur predominantly as the (oxy)hydroxide mineral gibbsite [$Al(OH)_3$] and boehmite (AlOOH).[2,30−32] Conversion of $Al(OH)_3$ into hydrated, crystalline sodium aluminates in concentrated NaOH at ambient temperatures has been used to process HLW at Hanford,[33,34] and recent work has shown that transformation from monosodium aluminate hydrate to nonasodium bis-(hexahydroxyaluminate) trihydroxide hexahydrate (NSA) proceeds spontaneously in the presence of excess sodium hydroxide monohydrate and water.[35] This highlights that the ongoing physical and chemical manipulation of these complex waste slurries, such as their removal from tanks and safe disposal in glass waste forms, requires the development of robust models that reliably predict phase equilibria and transformation kinetics.[36−38]

A variety of possible sodium aluminate hydroxy hydrate salts crystallize from these solutions (Figure 1A), which, like for the potassium and rubidium systems, may contain information about structural motifs present in solution because of their solid electrolyte characteristics.[39] For the current study, we selected NSA [$Na_9[Al(OH)_6]_2 \cdot 3(OH) \cdot 6(H_2O)$], a solid electrolyte hydrate containing monomeric Al^{3+} hydroxyanion octahedra ($Al(OH)_6^{3-}$) embedded in a matrix of edge-sharing Na^+ octahedra that are coordinated with water and hydroxyl ions (Figure 1B).[40,41] Because it is based on monomeric Al^{3+} octahedra, the precipitation of NSA can be regarded as a useful conceptual model for an intermediate Al^{3+} coordination state that is incipient to crystallization of polymerized octahedral Al^{3+} networks. Herein, we detail a μ-oxo sodium aluminate dimer [$Na_2Al_2O(OH)_6$] resolved in the caustic water-in-salt electrolyte, NSA, using ^{27}Al magic-angle spinning (MAS) NMR spectroscopy at high magnetic field strengths with supporting X-ray diffraction (XRD), scanning electron microscopy (SEM), Raman spectroscopy, and liquid-state ^{27}Al NMR. Description of $Na_2Al_2O(OH)_6$ advances the molecular-level understanding of both phase equilibria in the $Na_2O/Al_2O_3/H_2O$ system, and also transformations of Al^{3+} coordination as $Na_2Al_2O(OH)_6$ may exist as a reactive intermediate during solid-state crystallization under highly alkaline conditions, linking the soluble, tetrahedral aluminates to the solid-state, monomeric octahedral aluminate in NSA.

2. METHODS

2.1. Synthesis of NSA. All steps were performed in an N_2-filled glovebox to limit sorption of CO_2 and followed a previously published synthesis.[41] A 31.3 m aluminum-free NaOH solution was prepared in a wide-mouth polypropylene bottle from addition of H_2O (18 MΩ·cm) to NaOH (>98%, Sigma-Aldrich). Exothermic dissolution of NaOH increased the temperature of the NaOH solution to ca. 77 °C, and an aluminum wire (>99.999% grade, Sigma-Aldrich) was added to generate a 0.6 m Al^{3+} solution. Safety note: the dissolution of Al wire in NaOH solutions is exothermic and generates flammable H_2 gas. Following complete dissolution of the Al wire, the solution was placed in an oven at 40 °C, uncapped, for 2 days. After 2 days, the precipitated solids were collected via vacuum filtration to reduce the amount of residual mother liquor.

2.2. SEM. SEM micrographs were acquired with a Helios Nanolab 600i SEM (FEI, Hillsoboro, OR) microscope with an acceleration voltage of 20.00 kV and a current of 0.17 nA. NSA solids were placed on Al SEM stubs covered with a carbon tape in an N_2-filled glovebox and transported in a sealed container to the microscope for analysis.

2.3. ^{27}Al MAS NMR Spectroscopy. ^{27}Al MAS NMR spectroscopy was performed on a Bruker NMR spectrometer at a field strength of 14.1 T corresponding to a 156.375 MHz ^{27}Al Larmor frequency. Spectra were acquired with a MASDVT600W2 BL2.5 X/Y/H probe. Samples were loaded into commercial 2.5 mm Bruker rotors, equipped with a Vespel drive and bottom caps, in an N_2-filled glovebox. Single-pulse, direct excitation ^{27}Al MAS NMR spectra were acquired with ca. 49,000 and 2048 transients for $Na_9[Al(OH)_6]_2 \cdot 3(OH) \cdot 6(H_2O)$ and $K_2Al_2O(OH)_6$, respectively, and both samples utilized an acquisition time of 18.6 ms, a delay between transients of 1 s, and a single, $\pi/20$ liquid-state pulse. Tip angles were determined via a pulse width nutation experiment for a sample of 1 M $Al(H_2O)_6^{3+}$, prepared via dissolution of aluminum chloride hexahydrate ($AlCl_3 \cdot 6H_2O$, >99%, Sigma-Aldrich) in H_2O. Chemical shifts were also referenced to this 1 M $Al(H_2O)_6^{3+}$ solution in which the hexa-aqua aluminum ion resonance was set to 0 ppm. Spectra were primarily collected with a MAS spin rate of 20 kHz, and additional spectra were acquired under static conditions (0 kHz spin rate). MAS NMR spectra were processed in Mestrenova (version 14.01-23559, released 2019-06-07, Mestrelab Research S.L.). The free induction decay was zero-filled to 52.5 ms, and 20 Hz line broadening was applied. Line deconvolution was performed in

https://dx.doi.org/10.1021/acs.jpcc.0c00205
J. Phys. Chem. C 2020, 124, 12337−12345

DMFIT (release#20190327), where the line shape of the central transition was estimated with the Qmas 1/2 model.

Additional ^{27}Al MAS NMR spectra were acquired at a field strength of 20.0 T on a Varian NMR spectrometer, corresponding to a 221.517 MHz ^{27}Al Larmor frequency. A 1.6 mm MAS probe was used, operating at a spin rate of 20.0 kHz, and additional spectra were acquired for $Na_9[Al(OH)_6]_2 \cdot 3(OH) \cdot 6(H_2O)$ under static spinning rates (0 kHz). Chemical shifts and tip angles were referenced to a 1 M $Al(H_2O)_6^{3+}$ solution prepared via dissolution of aluminum nitrate nonahydrate ($Al(NO_3)_3 \cdot 9H_2O$, ≥98%, Sigma-Aldrich) in H_2O, in which the hexa-aqua aluminum ion resonance was set to 0 ppm. For acquisition of the $K_2Al_2O(OH)_6$ ^{27}Al MAS NMR spectra, a single excitation pulse corresponding to a liquid-state $\pi/20$ pulse, a delay between transients of 1 s, an acquisition time of 20 ms, and collection of 128 transients were used. Excitation pulse length nutation experiments utilized a delay of 3 s for $K_2Al_2O(OH)_6$. To facilitate detection of trace species in $Na_9[Al(OH)_6]_2 \cdot 3(OH) \cdot 6(H_2O)$, a single excitation pulse corresponding to a liquid-state $\pi/20$ pulse, a delay between transients of 1 s, an acquisition time of 20 ms, and an extensive collection of ca. 334,700 transients were used. Pulse nutation experiments of $Na_9[Al(OH)_6]_2 \cdot 3(OH) \cdot 6(H_2O)$, where the tetrahedral region is shown, used a delay between transients of 1 s. Pulse nutation experiments of $Na_9[Al(OH)_6]_2 \cdot 3(OH) \cdot 6(H_2O)$, where the octahedral region is shown, used a delay between transients of 3 s. Following acquisition, the spectra were analyzed in Mestrenova, where the free induction decay was zero-filled to 79 ms, and 20 Hz line broadening was applied. Line deconvolution was performed in DMFIT, where the central transition was estimated with the Qmas 1/2 model.

^{27}Al multiple quantum MAS (MQMAS) NMR spectra at a field strength of 20.0 T were acquired using a 1.6 mm MAS probe with the z-filter, ^{27}Al 3QMAS pulse sequence (mqmas3qzf2d) at a spinning rate of 20.0 kHz at a temperature of 20 °C. The optimized pulse widths, pw1Xmqmas, pw2Xmqmas, and pw3Xmqmas, were 3.75, 1.7, and 25 μs, respectively. The amplitude (aXmqmas) was 2500, the power (tpwr) was 56 dB, and the amplitude of the selective pulse (aXzfsel) was 250 with a corresponding power of 49 dB. The time between the second and third pulses (tXzfsel) was 10 μs. The recycle delay (d1) was 1 s, and spectra were acquired with 64 evolution increments, a 19.968 ms acquisition time, and 384 transients. The spectral widths for the F2 (acquisition) and F1 (evolution) dimensions were 166.7 and 20.0 kHz, respectively. The acquired spectrum was processed with 20 Hz line broadening in the F2 dimension and displayed after shearing.

^{27}Al MQMAS spectra at a field strength of 14.1 T were acquired using the Bruker 2.5 mm MAS probe with a z-filter, ^{27}Al 3QMAS pulse sequence (mp3qzqf) at a spinning rate of 20.0 kHz. The optimized pulse widths, P1, P2, and P3, were 4.6, 1.5, and 18 μs, respectively. The power level for the excitation pulse and conversion pulse was −20 dB, and the power level for the selective pulse was 5.23 dB. The time between the second and third pulses (D4) was 20 μs. The recycle delay (d1) was 40 s, and spectra were acquired with 74 evolution increments, a 17.8 ms acquisition time, and 24 transients. The spectral widths for the F2 (acquisition) and F1 (evolution) dimensions were 31.3 and 20.0 kHz, respectively. The acquisition utilized states-time proportional phase incrementation processing, and the two-dimensional spectrum was sheared in Topspin v(3.5.7).

2.4. Synthesis of $K_2Al_2O(OH)_6$. To generate a spectroscopy reference, the potassium μ-oxo aluminate dimer $[K_2Al_2O(OH)_6]$ was synthesized. All steps were performed in an N_2-filled glovebox to limit sorption of CO_2 following a previously reported synthesis.[8,20] An 18.7 m aluminum-free KOH solution was prepared in a fluorinated ethylene propylene (FEP) narrow-mouth bottle via dissolution of KOH (>99.98%, Alfa Aesar) in H_2O. After waiting for the solution to cool to about 20 °C, an aluminum wire was incrementally dissolved in the KOH solution such that the concentration of Al was 7.4 m Al. After dissolution of the Al wire, the bottle was capped, and the solution was left unagitated at 20 °C for 1 week. The formed crystals were collected via centrifugation at 8000 rpm and washed with anhydrous ethanol (Molecular Biology Grade, Fisher Scientific). The product was dried at 40 °C in an oven.

2.5. Liquid-State ^{27}Al NMR Spectroscopy. Liquid-state ^{27}Al NMR spectra were acquired on a Varian-Inova 17.6 T NMR spectrometer utilizing a 5 mm broadband observe probe operating at 40 °C, where the temperature was calibrated using the ^{1}H chemical shifts of ethylene glycol.[43] The corresponding ^{27}Al Larmor frequency is 195.460 MHz. Upon complete dissolution of 0.6 m Al wire in 31.3 m NaOH, an aliquot was placed in an uncapped, 4 mm outer diameter (o.d.) FEP copolymer insert. A reference solution [0.1 m $Al(OH)_4^-$ in 3 m NaOH, prepared via dissolution of Al wire in 3 m NaOH] was placed in a 2.0 mm o.d. FEP insert, sealed with a polytetrafluorethylene plug, and coaxially inserted inside the 4 mm FEP insert. The FEP inserts were then inserted into an uncapped N_2-filled 5.0 mm o.d. NMR tube and placed in the NMR spectrometer.

Sample acquisition utilized a single-pulse sequence (s2pul), in which free induction decays were collected with alternating excitation pulse lengths of $\pi/2$ and $\pi/20$, where the tip angles were referenced to the 0.1 m $Al(OH)_4^-$ in 3 m NaOH solution. The acquisition time was 0.600 s, the delay between scans was 2 s, and the acquisition used 24,194 complex points. For each one-dimensional spectrum, 128 transients were collected. Liquid-state NMR spectra were processed in Mestrenova where 20 Hz of line broadening was applied. Liquid-state NMR spectra were zero-filled to 65,536 points and baseline-corrected using spline functions, and the resonances were deconvoluted using a Lorentzian line shape.

2.6. Raman Spectroscopy. Raman spectra were acquired on aliquots taken from the mother liquor during precipitation. Data was collected on a Horiba LabRam HR spectrometer equipped on a Nikon Ti-E inverted microscope using a 40× microscope objective via application of a continuous 632.81 nm laser. Spectra were background-corrected with a single polynomial spanning between 500 and ca 800 cm^{-1}, and the resonances were deconvoluted using three Lorentzian line shapes.

3. RESULTS AND DISCUSSION

To enable detailed characterization of trace aluminates in NSA crystals via ^{27}Al MAS NMR, NSA crystals were synthesized under conditions indicated in Figure 1A. SEM images of crystallites precipitated from the mother liquor reveal their columnar crystal habit and average length of over a hundred microns (Figure 1C). The powder XRD pattern confirmed that the crystalline phases are predominantly NSA (75% relative abundance), coprecipitated with sodium hydroxide monohy-

https://dx.doi.org/10.1021/acs.jpcc.0c00205
J. Phys. Chem. C 2020, 124, 12337−12345

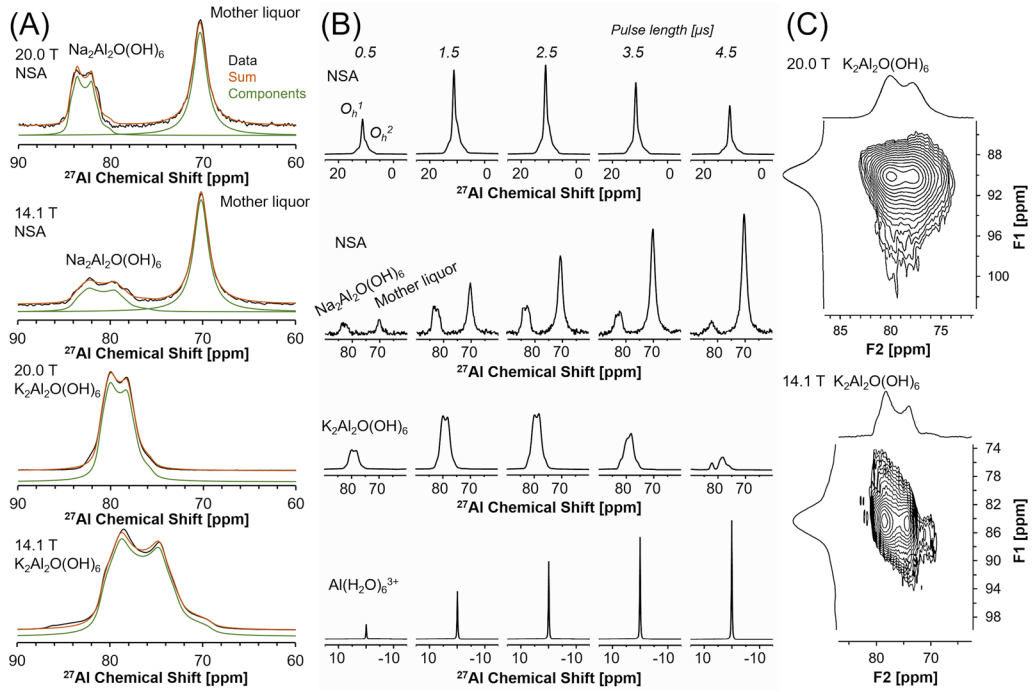

Figure 2. (A) ^{27}Al MAS NMR spectra at a field strength of 20.0 and 14.1 T showing that the tetrahedral coordinated Al^{3+} region spanning between 90 and 60 ppm in NSA is comparable to the resonance of $K_2Al_2O(OH)_6$. The deconvoluted quadrupolar line shape fits are vertically offset in green, the summed fits are shown in orange, and the data are shown in black. (B) Pulse length nutation experiments at 20.0 T, where incrementally increasing pulse durations are the same for each column and the spectra are shaded gray to guide the eyes. (C) ^{27}Al MQMAS NMR experiments of $K_2Al_2O(OH)_6$ at 20.0 and 14.1 T, where the F2 and F1 projections are summations.

Table 1. Quadrupolar Coupling Parameters for ^{27}Al MAS NMR[a]

field strength [T]	assignment	isotropic chemical shift [ppm]	quadrupolar coupling coefficient [MHz]	asymmetry parameter	line broadening [ppm]	integral [%]
14.1	$Na_2Al_2O(OH)_6$	84.6	3.8	0.3	1.1	0.6
20.0	$Na_2Al_2O(OH)_6$	84.9	4.0	0.3	0.4	0.4
14.1	$K_2Al_2O(OH)_6$	81.9	4.5	0.3	1.3	100
20.0	$K_2Al_2O(OH)_6$	81.6	4.5	0.3	0.9	100

[a]Note: quadrupolar line shapes were calculated in DMFIT (release #20180327) and utilized the Qmas 1/2 model, which assumes infinite spinning rates. The quadrupolar line fit for resonances corresponding to the octahedral coordinated Al^{3+} in NSA is shown in Figure S3, with the quadrupolar coupling parameters detailed in Table S1.

drate ($NaOH{\cdot}H_2O$, 25% relative abundance) shown in Figure S1.

The speciation of Al^{3+} ions in these solids was analyzed using ^{27}Al MAS NMR, which is selective to Al^{3+} in the NSA phase and any residual form of Al^{3+} species associated with the solids. The high natural abundance (100%) and sensitivity of the ^{27}Al MAS NMR chemical shift to the coordination environment about the Al^{3+} nucleus[44] enables, for example, any tetrahedrally coordinated Al^{3+} species associated with the solids to be distinguished from the monomeric Al^{3+} hydroxyanion octahedra in NSA. ^{27}Al MAS NMR spectra showing the two predominant Al^{3+} sites of the monomeric Al^{3+} hydroxyanion octahedra in NSA are shown in Figure S2. Magnification of the ^{27}Al MAS NMR spectra at both field strengths of 14.1 and 20.0 T reveals two tetrahedral resonances at approximately 80 and 70 ppm (Figure 2) in the NSA crystals. The primary goal of this work is to exploit detailed ^{27}Al MAS NMR characterization, with supporting liquid-state NMR and Raman spectroscopies, to characterize and identify these tetrahedral species.

The tetrahedral Al^{3+} resonance in the solids occurring at ca. 80 ppm is denoted $Na_2Al_2O(OH)_6$ because it exhibits a quadrupolar line shape similar to that for a separately synthesized crystalline potassium aluminate $K_2Al_2O(OH)_6$ standard.[20] The quadrupolar line shape, evaluated using the Qmas 1/2 model in DMFIT, is shown in Figure 2. The similar electron field gradient asymmetry (η) and quadrupolar coupling (C_Q) parameters demonstrate likely conservation of the $Al_2O(OH)_6^{2-}$ motif, and the regressed values are described in Table 1.

Importantly, a substantial reduction in the breadth of both $Na_2Al_2O(OH)_6$ and $K_2Al_2O(OH)_6$ resonances was observed in ^{27}Al MAS NMR spectra upon increasing the field strength to 20.0 T, indicating that second-order quadrupolar effects are significant. This suggests that chemical moieties of the Al^{3+} ligands are asymmetric, as is the case for $Al_2O(OH)_6^{2-}$.[45] The dependence of the ^{27}Al line shape on the magnetic field strength would not be apparent for a crystalline $Al(OH)_4^-$ monomer, based on the quasi-Lorentzian line shape acquired with ^{27}Al MAS NMR of $Na_2Al(OH)_4Cl$, at 9.4 T.[46] A key difference between $Na_2Al_2O(OH)_6$ and $K_2Al_2O(OH)_6$ arises

https://dx.doi.org/10.1021/acs.jpcc.0c00205
J. Phys. Chem. C 2020, 124, 12337−12345

in the isotropic chemical shift, which can be attributed to a combination of Na^+/K^+ specific ion effects, slight perturbation of the Al−O−Al angle, and/or formation of a hydrated phase. The isotropic chemical shift of the $Na_2Al_2O(OH)_6$ resonance is significantly deshielded compared to oxolated tetrahedral Al^{3+} proximal to octahedral Al^{3+}, such as in keggin clusters or transitional aluminas.[47−52]

Significant quadrupolar effects in both $Na_2Al_2O(OH)_6$ and the $K_2Al_2O(OH)_6$ standard are also evident in the excitation pulse length nutation experiment shown at a field strength of 20 T in Figure 2B. The pulse length nutation experiment demonstrates that the signal maxima of $Na_2Al_2O(OH)_6$ occurs upon a shorter pulse duration than that for the resonance of the hexa-aqua aluminum ion $[Al(H_2O)_6^{3+}]$. Crucially, molecular tumbling of $Al(H_2O)_6^{3+}$ eliminates quadrupolar coupling. Vice-a-versa, the retention of quadrupolar coupling effects in $Na_2Al_2O(OH)_6$ suggests its presence in interstitial sites or on the surface of the solids. Relative to $Al(H_2O)_6^{3+}$ pulse nutation behavior, the crystalline $K_2Al_2O(OH)_6$ standard also exhibits a reduced pulse length corresponding to the maximum signal response. This similar pulse nutation behavior between $Na_2Al_2O(OH)_6$ and the $K_2Al_2O(OH)_6$ standard further supports attributing the $Na_2Al_2O(OH)_6$ resonance to a solid phase. Analysis of the nutation curve of the two monomeric framework octahedra Al^{3+} in NSA crystals (O_h^1 and O_h^2), ca 10 ppm, also demonstrates a reduced pulse length maximum relative to $Al(H_2O)_6^{3+}$.

Given the strong resemblance of the quadrupolar ^{27}Al MAS NMR line shape of the $Al_2O(OH)_6^{2-}$ motif in the $K_2Al_2O(OH)_6$ standard and the trace resonance in the NSA crystals, MQMAS NMR spectroscopy was conducted to provide NMR spectra with greater resolution, with results shown in Figure 2C. In MQMAS NMR spectroscopy, multiple quantum coherences are first excited and then converted into single-quantum coherence.[53] Correlation of the multiple- and single-quantum coherences through two-dimensional NMR experiments facilitates separation of chemically inequivalent sites by their isotropic quadrupolar shifts and isotropic chemical shift.[53,54] Given the low abundance of $Na_2Al_2O(OH)_6$ and the poor coherence transfer efficiency in MQMAS NMR scans, the ^{27}Al MQMAS NMR spectra of $K_2Al_2O(OH)_6$ was instead acquired at 14.1 and 20.0 T to provide insight into the $Al_2O(OH)_6^{2-}$ resonance associated with the NSA crystalline solids.

The acquired ^{27}Al MQMAS NMR spectra shown in Figure 2C show a single projection in the F1 dimension at both field strengths. This demonstrates that $K_2Al_2O(OH)_6$ is purely composed of Al^{3+} existing in one crystallographically unique site and is consistent with the crystal structure derived from single-crystal XRD.[7] ^{27}Al MQMAS NMR of $K_2Al_2O(OH)_6$ validates that its complex ^{27}Al MAS NMR spectra arises from quadrupolar coupling influencing a single Al^{3+} site and not from the superposition of many Al^{3+} sites. Given the comparable quadrupolar coupling parameters and line shape dependence on the magnetic field strength between $K_2Al_2O(OH)_6$ and $Na_2Al_2O(OH)_6$, the later resonance is also likely due to a single Al^{3+} site.

Following the description of the first tetrahedral species, the second tetrahedral coordinated Al^{3+} species in the NSA solids is described. The species exhibits a quasi-Lorentzian resonance which occurs at 70 ppm and is denoted as mother liquor in Figure 2. The chemical shift is shielded relative to the expected chemical shift of 80 ppm expected for $Al(OH)_4^-$ in dilute NaOH.[1,55] Analysis of the excitation pulse length nutation experiment supports assigning the quasi-Lorentzian resonance to residual mother liquor. Molecular tumbling of aluminate species in the liquid state eliminates quadrupolar coupling, resulting in the intensity of quadrupolar resonances exhibiting sinusoidal dependence on the applied excitation pulse length (Figure S4). The quasi-spin 1/2 behavior is comparable to $Al(H_2O)_6^{3+}$ in H_2O, as shown in Figure 2B. Comparison with nonspinning ^{27}Al MAS NMR spectra (Figure S2) demonstrates that the resonance exhibits a significantly smaller change in full width at half-maximum (fwhm) (800−300 Hz at 14.1 T and 900−400 Hz at 20.0 T) than the octahedral Al^{3+} in NSA upon spinning, which also supports assignment of this resonance to Al^{3+} in residual mother liquor.

To provide further insight into the resonance assigned to the Al^{3+} ions in the mother liquor, Al^{3+} ion speciation in the mother liquor during the synthesis procedure was examined via NMR and Raman spectroscopies during NSA crystallization. Starting with a fresh preparation of 0.6 m Al^{3+} in 31.3 m NaOH, crystallization of NSA was monitored in situ over the course of 2 days using single-pulse acquisition of ^{27}Al NMR spectra utilizing alternating $\pi/2$ and $\pi/20$ excitation tip angles. High-field (17.6 T) solution-state ^{27}Al NMR spectra are shown in Figure 3, where the resonance near 70 ppm is attributed to

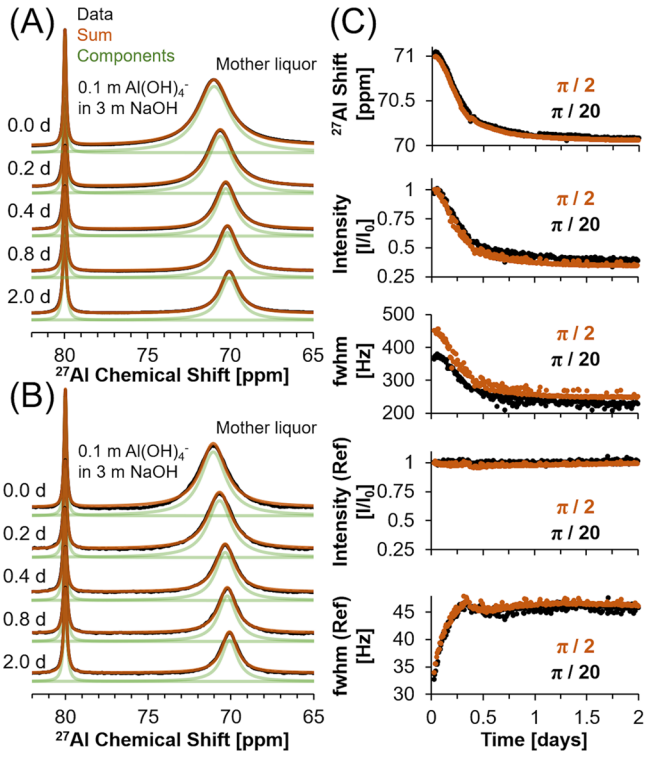

Figure 3. Time-dependent, 17.6 T, solution-state ^{27}Al NMR spectra during NSA crystallization acquired with (A) $\pi/2$, (B) $\pi/20$ excitation pulses, and (C) line deconvolution parameters. Additional solution-state ^{27}Al NMR spectra are shown in Figure S5.

the tetrahedral coordination of the aluminate species in the mother liquor. A sealed, coaxial insert containing a dilute solution of $Al(OH)_4^-$ ions in NaOH (0.1 m Al in 3 m NaOH) was used as a chemical shift reference at 80 ppm and as an intensity reference.[52] Throughout the crystallization of NSA, neither additional resonances in the octahedral region nor tetrahedral region emerge (Figure S5). An additional control

https://dx.doi.org/10.1021/acs.jpcc.0c00205
J. Phys. Chem. C 2020, 124, 12337−12345

experiment (Figure S6) validated that there is no emerging Al^{3+} resonance within the mother liquor that overlaps with the coaxial reference.

The sole ^{27}Al resonance of aluminates in the mother liquor is progressively shielded during crystallization, decreasing from 71 to 70 ppm, with the final resonance in close agreement with the quasi-Lorentzian resonance chemical shift found at ca. 70 ppm in the ^{27}Al MAS NMR spectra of the NSA crystals (Figure 2A) assigned to the mother liquor.

Irrespective of using an excitation pulse resulting in a $\pi/20$ or $\pi/2$ tip angle, the normalized integral of Al^{3+} in the mother liquor practically identically decreases from ca. 1.0 to 0.4 over the course of 2 days. The decrease in the integral of Al^{3+} in the mother liquor solution, shown in Figure 3C, indicates that crystallization of NSA proceeds at 40 °C over 2 days. The near perfect agreement between the normalized integrated intensity after $\pi/20$ and $\pi/2$ excitation pulses validates that the resonances are in the fast-motional limit, leading to the aluminates in the mother liquor exhibiting quasi-spin 1/2 behavior, in agreement with the behavior of the quasi-Lorentzian line shape at ca. 70 ppm found in the ^{27}Al MAS NMR spectra (Figures 2B and S4). Whereas the mother liquor ^{27}Al NMR resonance exhibits a significant decrease in fwhm over time, arising from quadrupolar relaxation convoluted with viscosity-dependent reorientation times, there is also an anticorrelated increase in the fwhm of the internal standard, likely due to the magnetic field inhomogeneity arising from crystallization of NSA.

Despite demonstrating the similar chemical shift and pulse length nutation behavior between the aluminates in the mother liquor and the residual quasi-Lorentzian line found in the ^{27}Al MAS NMR spectra, distinction between solution-state $Al(OH)_4^-$ and $Al_2O(OH)_6^{2-}$ by solution-state ^{27}Al NMR is expectedly complicated by fast hydrolysis and interconversion of Al^{3+} between $Al(OH)_4^-$ and $Al_2O(OH)_6^{2-}$, leading to coalescence into a single, ensemble resonance.

Therefore, Raman spectroscopy was performed to validate the presence of solution-state $Al_2O(OH)_6^{2-}$ ions during NSA crystallization (Figure 4) and to support the assignment of the trace tetrahedral quadrupolar line shape to $Na_2Al_2O(OH)_6$. During the crystallization of NSA, aliquots of the mother liquor were taken to generate a temporal series of Raman spectra. A stacked plot of the temporal progression of the mother liquor during crystallization is shown in Figure 4. The center band at ca. 625 cm^{-1} is assigned to Al−OH stretching for $Al(OH)_4^-$.[23,24,42] A shift of 4.4 cm^{-1} from 623.9 to 628.3 cm^{-1} occurs between the 0.3 m $Al(OH)_4^-$ in 3 m NaOH reference and the mother liquor, indicating the increased formation of $NaAl(OH)_4$ ion pairs in the mother liquor.[2,55,56] At 31.3 m NaOH, limited waters of solvation and geometric packing constraints likely result in the formation of hydrated ion networks in contrast to the weak formation of solvent-separated ion pairs under more dilute conditions.[2,19]

Based on the similarity between Raman spectra of solid $K_2Al_2O(OH)_6$ and MOH (M^+ = Na^+, K^+, Cs^+, or Rb^+) aluminate solutions,[8] the flanking bands at 568 and 701 cm^{-1} in Figure 4 are, respectively, assigned to the Al−μO and the Al−tOH vibrational modes of solution-state $Al_2O(OH)_6^{2-}$. Notably, these additional bands are essentially nonexistent in the 0.3 m $Al(OH)_4^-$ in 3 m NaOH reference solution. Deconvolution with Lorentzian line shapes indicates that despite the observed decrease in the total vibrational intensity, the relative intensity of the center band (ca. 628 cm^{-1})

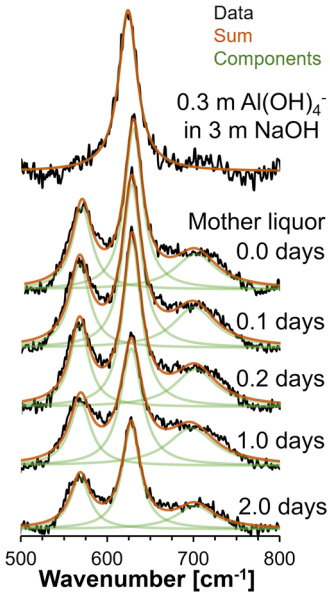

Figure 4. Deconvoluted Raman of the mother liquor and comparison with 0.3 m $Al(OH)_4^-$ in 3 m NaOH. A table of the line shape parameters is provided in Table S2 in the Supporting Information. The ratio of integrated intensity between the center band ca. 625 cm^{-1} and the flanking side bands at 568 and 701 cm^{-1} remains ca. 1:1, despite the decrease in intensity following Al^{3+} crystallization.

attributed to monomers insignificantly increases from 49.3 to 50.8% during crystallization. There is no significant increase in the relative $Al_2O(OH)_6^{2-}$ signals, which would be expected for pure evaporation without NSA crystallization, based upon extrapolation of the negative correlation between the relative $Al_2O(OH)_6^{2-}$ signal and the amount of water present in solution at the molar ratio Na^+/Al^{3+} = 52:1 (Figure S7). However, in addition to a decrease in water activity through evaporation, there is also a reduction in the solution-phase Al^{3+} and other ions during crystallization of NSA. These Raman results clearly indicate that the $Al_2O(OH)_6^{2-}$ ions are prevalent in the mother liquor and remain so during precipitation of NSA, and that these solution phase species coincide with the observation of $Na_2Al_2O(OH)_6$ in ^{27}Al MAS NMR spectra of the NSA solids.

4. CONCLUSIONS

Characterization of trace, residual Al^{3+} species that have evaded spectroscopic detection via ^{27}Al NMR until now provides significant new insights into the $Na_2O/Al_2O_3/H_2O$ system and more generally demonstrates an extension of the complexity of crystal growth from monomeric and oligomeric precursors[57] to highly alkaline solutions. Recognition of the presence and persistence of $Al_2O(OH)_6^{2-}$ during crystallization in the $Na_2O/Al_2O_3/H_2O$ system establishes a link to known solution speciation behavior of other highly alkaline systems, such as potassium and rubidium hydroxide solutions. This demonstrates that NSA crystallizes from a solution in which Al^{3+} is present as both tetrahedrally coordinated $Al(OH)_4^-$ and $Al_2O(OH)_6^{2-}$ species that persist as trace residuals on or within product NSA crystallites. The depravation of water within the ion−ion networks in the crystallizing mother liquor creates a unique chemical environment, where release of water via condensation of $Al(OH)_4^-$ units leads to a perturbed tetrahedral $Al_2O(OH)_6^{2-}$ species

https://dx.doi.org/10.1021/acs.jpcc.0c00205
J. Phys. Chem. C 2020, 124, 12337−12345

that ultimately precipitates and appears as a residual in the crystalline products. It remains unclear whether these species are incorporated as trace defects in remnant $NaOH{\cdot}H_2O$, are interstitials in NSA, or represent a metastable state on the NSA surface. However, this observation of $Na_2Al_2O(OH)_6$ is coupled with the notable absence of both solid-state monomeric tetrahedra, for example, $NaAl(OH)_4$, and liquid-state monomeric octahedra, for example, $Al(OH)_6^{3-}$. Such observations indicate that the Al^{3+} coordination change occurs either on the NSA crystal surface or during a solid-state amorphous-to-crystalline transition but not in solution. Given that the isolation of $Na_2Al_2O(OH)_6$ has eluded many others exploring the $Na_2O/Al_2O_3/H_2O$ phase space,[10−17] it is reasonable to infer from the instability of $Na_2Al_2O(OH)_6$ that it may exist as a reactive intermediate during solid-state crystallization, linking the soluble tetrahedral aluminates under highly alkaline conditions to the monomeric octahedra in NSA. Further isolation of crystallization pathways, including the prospect of solid-state transformation, is underway to better understand Al^{3+} coordination change mechanisms in caustic environments relevant to myriad process applications.

■ ASSOCIATED CONTENT

Supporting Information

The Supporting Information is available free of charge at https://pubs.acs.org/doi/10.1021/acs.jpcc.0c00205.

X-ray diffraction of NSA, ^{27}Al MAS NMR spectra, quadrupolar coupling parameters for ^{27}Al MAS NMR spectra, ^{27}Al MAS NMR pulse length nutation experiments, liquid-state ^{27}Al NMR results, additional Raman spectroscopy results, and line shape parameters for Raman spectra of the mother liquor (PDF)

■ AUTHOR INFORMATION

Corresponding Authors

Trent R. Graham − *Physical and Computational Sciences Directorate, Pacific Northwest National Laboratory, Richland, Washington 99354, United States;* orcid.org/0000-0001-8907-8004; Email: trenton.graham@pnnl.gov

Kevin M. Rosso − *Physical and Computational Sciences Directorate, Pacific Northwest National Laboratory, Richland, Washington 99354, United States;* orcid.org/0000-0002-8474-7720; Email: Kevin.rosso@pnnl.gov

Authors

Mateusz Dembowski − *Physical and Computational Sciences Directorate, Pacific Northwest National Laboratory, Richland, Washington 99354, United States;* orcid.org/0000-0002-6665-8417

Jian Zhi Hu − *Physical and Computational Sciences Directorate and Institute for Integrated Catalysis, Pacific Northwest National Laboratory, Richland, Washington 99354, United States;* orcid.org/0000-0001-8879-747X

Nicholas R. Jaegers − *Physical and Computational Sciences Directorate and Institute for Integrated Catalysis, Pacific Northwest National Laboratory, Richland, Washington 99354, United States; The Voiland School of Chemical and Biological Engineering, Washington State University, Pullman, Washington 99164, United States;* orcid.org/0000-0002-9930-7672

Xin Zhang − *Physical and Computational Sciences Directorate, Pacific Northwest National Laboratory, Richland, Washington 99354, United States;* orcid.org/0000-0003-2000-858X

Sue B. Clark − *Energy and Environment Directorate, Pacific Northwest National Laboratory, Richland, Washington 99354, United States; Department of Chemistry, Washington State University, Pullman, Washington 99164, United States*

Carolyn I. Pearce − *Energy and Environment Directorate, Pacific Northwest National Laboratory, Richland, Washington 99354, United States;* orcid.org/0000-0003-3098-1615

Complete contact information is available at: https://pubs.acs.org/10.1021/acs.jpcc.0c00205

Notes

The authors declare no competing financial interest.

■ ACKNOWLEDGMENTS

This research was supported by IDREAM (Interfacial Dynamics in Radioactive Environments and Materials), an Energy Frontier Research Center funded by the U.S. Department of Energy (DOE), Office of Science, Basic Energy Sciences (BES). SEM, XRD, and NMR and Raman spectroscopies were performed using the facilities at the Environmental Molecular Science Laboratory (EMSL, grid. 436923.9), a DOE Office of Science User Facility sponsored by the Office of Biological and Environmental Research at the Pacific Northwest National Laboratory (PNNL). PNNL is a multiprogram national laboratory operated for DOE by the Battelle Memorial Institute operating under contract no. DE-AC05-76RL0-1830. The 14.1 T NMR spectrometer was acquired with support from the BES Chemical Sciences, Geochemistry, & Biosciences (CSGB) Division.

■ REFERENCES

(1) Sipos, P. The Structure of Al(III) in Strongly Alkaline Aluminate Solutions − A Review. *J. Mol. Liq.* **2009**, *146*, 1−14.

(2) Graham, T. R.; Dembowski, M.; Martinez-Baez, E.; Zhang, X.; Jaegers, N. R.; Hu, J.; Gruszkiewicz, M. S.; Wang, H.-W.; Stack, A. G.; Bowden, M. E.; et al. In Situ ^{27}Al NMR Spectroscopy of Aluminate in Sodium Hydroxide Solutions above and below Saturation with Respect to Gibbsite. *Inorg. Chem.* **2018**, *57*, 11864−11873.

(3) Shen, Z.; Kerisit, S. N.; Stack, A. G.; Rosso, K. M. Free-Energy Landscape of the Dissolution of Gibbsite at High pH. *J. Phys. Chem. Lett.* **2018**, *9*, 1809−1814.

(4) Eggleston, C. M.; Stack, A. G.; Rosso, K. M.; Bice, A. M. Adatom Fe(III) on the Hematite Surface: Observation of a Key Reactive Surface Species. *Geochem. Trans.* **2004**, *5*, 33−40.

(5) Dembowski, M.; Snyder, M. M.; Delegard, C. H.; Reynolds, J. G.; Graham, T. R.; Wang, H.-W.; Leavy, I. I.; Baum, S. R.; Qafoku, O.; Fountain, M. S.; et al. Ion−Ion Interactions Enhance Aluminum Solubility in Alkaline Suspensions of Nano-Gibbsite (α-$Al(OH)_3$) with Sodium Nitrite/Nitrate. *Phys. Chem. Chem. Phys.* **2020**, *22*, 4368.

(6) Wang, H.-W.; Graham, T. R.; Mamontov, E.; Page, K.; Stack, A. G.; Pearce, C. I. Countercations Control Local Specific Bonding Interactions and Nucleation Mechanisms in Concentrated Water-in-Salt Solutions. *J. Phys. Chem. Lett.* **2019**, *10*, 3318−3325.

(7) Johansson, G.; Hope, H.; Nevald, R.; Frank, V.; Brunvoll, J.; Bunnenberg, E.; Djerassi, C.; Records, R. The Crystal Structure of Potassium Aluminate $K_2[Al_2O(OH)_6]$. *Acta Chem. Scand.* **1966**, *20*, 505−515.

(8) Moolenaar, R. J.; Evans, J. C.; McKeever, L. D. Structure of the Aluminate Ion in Solutions at High pH. *J. Phys. Chem.* **1970**, *74*, 3629−3636.

(9) Ivlieva, V. I.; Ivanov-Emin, B. N.; Kaziev, G. Z.; Yu, G. T. X-Ray Diffraction Investigation of Rubidium Hydroxoaluminate and Hydroxogallate. *Zh. Neorg. Khim.* **1980**, *25*, 1107.

(10) Zhang, Y.; Li, Y.; Zhang, Y. Phase Diagram for the System Na_2O-Al_2O_3-H_2O at High Alkali Concentration. *J. Chem. Eng. Data* **2003**, *48*, 617−620.
(11) Ma, S.; Zheng, S.; Zhang, Y.; Zhang, Y. Phase Diagram for the Na_2O-Al_2O_3-H_2O System at 130°C. *J. Chem. Eng. Data* **2007**, *52*, 77−79.
(12) Bourcier, W. L.; Knauss, K. G.; Jackson, K. J. Aluminum Hydrolysis Constants to 250°C from Boehmite Solubility Measurements. *Geochim. Cosmochim. Acta* **1993**, *57*, 747−762.
(13) Wesolowski, D. J. Aluminum Speciation and Equilibria in Aqueous Solution: I. The Solubility of Gibbsite in the System Na-K-Cl-OH-Al(OH)4 from 0 to 100°C. *Geochim. Cosmochim. Acta* **1992**, *56*, 1065−1091.
(14) Sprauer, J. W.; Pearce, D. W. Equilibria in the Systems Na_2O−SiO_2−H_2O and Na_2O−Al_2O_3−H_2O at 25°C. *J. Phys. Chem.* **1940**, *44*, 909.
(15) Weinberger, M.; Schneider, M.; Geßner, W. H.; Müller, D. Die Kristallstruktur Des Natriumoxohydroxoaluminathydrates $Na_2[Al_2O_3(OH)_2]\cdot 1{,}5H_2O$. *Z. Anorg. Allg. Chem.* **1995**, *621*, 679.
(16) Qiu, G.; Chen, N. Phase Study of the System Na_2O-Al_2O_3-H_2O. *Can. Metall. Q.* **1997**, *36*, 111−114.
(17) Gessner, W.; Weinberger, M.; Müller, D.; Ni, L. P.; Chaljapina, O. B. Zur Kenntnis Der Kristallinen Phasen in Den Systemen M_2O-Al_2O_3-H_2O (M = K, Na). *Z. Anorg. Allg. Chem.* **1987**, *547*, 27.
(18) Graham, T. R.; Semrouni, D.; Mamontov, E.; Ramirez-Cuesta, A. J.; Page, K.; Clark, A.; Schenter, G. K.; Pearce, C. I.; Stack, A. G.; Wang, H.-W. Coupled Multimodal Dynamics of Hydrogen-Containing Ion Networks in Water-Deficient, Sodium Hydroxide-Aluminate Solutions. *J. Phys. Chem. B* **2018**, *122*, 12097−12106.
(19) Graham, T. R.; Han, K. S.; Dembowski, M.; Krzysko, A. J.; Zhang, X.; Hu, J.; Clark, S. B.; Clark, A. E.; Schenter, G. K.; Pearce, C. I.; et al. ^{27}Al Pulsed Field Gradient, Diffusion-NMR Spectroscopy of Solvation Dynamics and Ion Pairing in Alkaline Aluminate Solutions. *J. Phys. Chem. B* **2018**, *122*, 10907−10912.
(20) Pouvreau, M.; Dembowski, M.; Clark, S. B.; Reynolds, J. G.; Rosso, K. M.; Schenter, G. K.; Pearce, C. I.; Clark, A. E. Ab Initio Molecular Dynamics Reveal Spectroscopic Siblings and Ion Pairing as New Challenges for Elucidating Prenucleation Aluminum Speciation. *J. Phys. Chem. B* **2018**, *122*, 7394−7402.
(21) Wildman, A.; Martinez-Baez, E.; Fulton, J.; Schenter, G.; Pearce, C.; Clark, A. E.; Li, X. Anticorrelated Contributions to Pre-Edge Features of Aluminate Near-Edge X-Ray Absorption Spectroscopy in Concentrated Electrolytes. *J. Phys. Chem. Lett.* **2018**, *9*, 2444−2449.
(22) Buchner, R.; Sipos, P.; Hefter, G.; May, P. M. Dielectric Relaxation of Concentrated Alkaline Aluminate Solutions. *J. Phys. Chem. A* **2002**, *106*, 6527−6532.
(23) Johnston, C. T.; Agnew, S. F.; Schoonover, J. R.; Kenney, J. W.; Page, B.; Osborn, J.; Corbin, R. Raman Study of Aluminum Speciation in Simulated Alkaline Nuclear Waste. *Environ. Sci. Technol.* **2002**, *36*, 2451−2458.
(24) Schoonover, J. R.; Zhang, S. L.; Johnston, C. T. Raman Spectroscopy and Multivariate Curve Resolution of Concentrated Al_2O_3-Na_2O-H_2O Solutions. *J. Raman Spectrosc.* **2003**, *34*, 404−412.
(25) Buvári-barcza, Á.; Rózsahegyi, M.; Barcza, L. Hydrogen Bonded Associates in the Bayer Process (in Concentrated Aluminate Lyes): The Mechanism of Gibbsite Nucleation. *J. Mater. Chem.* **1998**, *8*, 451−455.
(26) Li, X.-b.; Yan, L.; Zhou, Q.-s.; Liu, G.-h.; Peng, Z.-h. Thermodynamic Model for Equilibrium Solubility of Gibbsite in Concentrated NaOH Solutions. *Trans. Nonferrous Met. Soc. China* **2012**, *22*, 447−455.
(27) Zhang, J.; Klasky, M.; Letellier, B. C. The Aluminum Chemistry and Corrosion in Alkaline Solutions. *J. Nucl. Mater.* **2009**, *384*, 175−189.
(28) Reynolds, J. G.; McCoskey, J. K.; Herting, D. L. Gibbsite Solubility in Hanford Nuclear Waste Approached from above and below Saturation. *Ind. Eng. Chem. Res.* **2016**, *55*, 5465−5473.
(29) Peterson, R. A.; Buck, E. C.; Chun, J.; Daniel, R. C.; Herting, D. L.; Ilton, E. S.; Lumetta, G. J.; Clark, S. B. Review of the Scientific Understanding of Radioactive Waste at the U.S. DOE Hanford Site. *Environ. Sci. Technol.* **2018**, *52*, 381−396.
(30) Zhang, X.; Zhang, X.; Graham, T. R.; Pearce, C. I.; Mehdi, B. L.; N'Diaye, A. T.; Kerisit, S.; Browning, N. D.; Clark, S. B.; Rosso, K. M. Fast Synthesis of Gibbsite Nanoplates and Process Optimization Using Box-Behnken Experimental Design. *Cryst. Growth Des.* **2017**, *17*, 6801−6808.
(31) Zhang, X.; Huestis, P. L.; Pearce, C. I.; Hu, J. Z.; Page, K.; Anovitz, L. M.; Aleksandrov, A. B.; Prange, M. P.; Kerisit, S.; Bowden, M. E.; et al. Boehmite and Gibbsite Nanoplates for the Synthesis of Advanced Alumina Products. *ACS Appl. Nano Mater.* **2018**, *1*, 7115−7128.
(32) Zhang, X.; Cui, W.; Page, K. L.; Pearce, C. I.; Bowden, M. E.; Graham, T. R.; Shen, Z.; Li, P.; Wang, Z.; Kerisit, S.; et al. Size and Morphology Controlled Synthesis of Boehmite Nanoplates and Crystal Growth Mechanisms. *Cryst. Growth Des.* **2018**, *18*, 3596−3606.
(33) Herting, D. L.; Reynolds, J. G.; Barton, W. B. Conversion of Coarse Gibbsite Remaining in Hanford Nuclear Waste Tank Heels to Solid Sodium Aluminate $[NaAl(OH)_4\cdot 1.5H_2O]$. *Ind. Eng. Chem. Res.* **2014**, *53*, 13833−13842.
(34) Chamberlain, B. E. *Assessment of 241-C-Farm Hard-Heel Retrievals Using Caustic Cleaning*: Richland, 2013.
(35) Graham, T. R.; Gorniak, R.; Dembowski, M.; Zhang, X.; Clark, S. B.; Pearce, C. I.; Clark, A. E.; Rosso, K. M. Solid-State Recrystallization Pathways of Sodium Aluminate Hydroxy Hydrates. *Inorg. Chem.***2020**, *5968576865*.
(36) Goel, A.; McCloy, J. S.; Pokorny, R.; Kruger, A. A. Challenges with Vitrification of Hanford High-Level Waste (HLW) to Borosilicate Glass − An Overview. *J. Non-Cryst. Solids* **2019**, *4*, 100033.
(37) Haverlock, T. J.; Bonnesen, P. V.; Moyer, B. A. Separation of NaOH by Solvent Extraction Using Weak Hydroxy Acids. *Solvent Extr. Ion Exch.* **2003**, *21*, 483−504.
(38) Moyer, B. A.; Custelcean, R.; Hay, B. P.; Sessler, J. L.; Bowman-James, K.; Day, V. W.; Kang, S.-O. A Case for Molecular Recognition in Nuclear Separations: Sulfate Separation from Nuclear Wastes. *Inorg. Chem.* **2013**, *52*, 3473−3490.
(39) Dillon, S. R.; Dougherty, R. C. Raman Studies of the Solution Structure of Univalent Electrolytes in Water. *J. Phys. Chem. A* **2002**, *106*, 7647−7650.
(40) Weinberger, M.; Schneider, M.; Zabel, V.; Müller, D.; Geßner, W. Nonanatrium-Bis(Hexahydroxoaluminat)-Trihydroxid-Hexahydrat $(Na_9[Al(OH)_6]_2(OH)_3\cdot 6H_2O)$ - Kristallstruktur, NMR-Spektroskopie Und Thermisches Verhalten. *Z. Anorg. Allg. Chem.* **1996**, *622*, 1799−1805.
(41) Zabel, V.; Schneider, M.; Weinberger, M.; Gessner, W. Nonasodium Bis(Hexahydroxoaluminate) Trihydroxide Hexahydrate. *Acta Crystallogr., Sect. C: Cryst. Struct. Commun.* **1996**, *52*, 747−749.
(42) Stephen, A.; Johnston, C. *Microstructural Properties of High Level Waste Concentrates and Gels with Raman and Infrared Spectroscopies*, 1997. DOE Report Number: 99-3332.
(43) Raiford, D. S.; Fisk, C. L.; Becker, E. D. Calibration of Methanol and Ethylene Glycol Nuclear Magnetic Resonance Thermometers. *Anal. Chem.* **1979**, *51*, 2050−2051.
(44) Akitt, J. W. Multinuclear Studies of Aluminium Compounds. *Prog. Nucl. Magn. Reson. Spectrosc.* **1989**, *21*, 1−149.
(45) Dec, S. F.; Maciel, G. E.; Fitzgerald, J. J. Solid-state sodium-23 and aluminum-27 MAS NMR study of the dehydration of sodium aluminate hydrate (Na2O.cntdot.Al2O3.cntdot.3H2O). *J. Am. Chem. Soc.* **1990**, *112*, 9069−9077.
(46) Weinberger, M.; Schneider, M.; Müller, D.; Geßner, W.; Reck, G. Zur Kenntnis Des Natrium-Tetrahydroxoaluminat-Chlorids $Na_2[Al(OH)_4]Cl$. *Z. Anorg. Allg. Chem.* **1994**, *620*, 771−776.
(47) Chandran, C. V.; Kirschhock, C. E. A.; Radhakrishnan, S.; Taulelle, F.; Martens, J. A.; Breynaert, E. Alumina: Discriminative

Analysis Using 3D Correlation of Solid-State NMR Parameters. *Chem. Soc. Rev.* **2019**, *48*, 134−156.
(48) Müller, D.; Gessner, W.; Samoson, A.; Lippmaa, E.; Scheler, G. Solid-State Aluminium-27 Nuclear Magnetic Resonance Chemical Shift and Quadrupole Coupling Data for Condensed AlO_4 Tetrahedra. *J. Chem. Soc., Dalton Trans.* **1986**, 1277−1281.
(49) Deschaume, O.; Breynaert, E.; Radhakrishnan, S.; Kerkhofs, S.; Haouas, M.; Adam De Beaumais, S.; Manzin, V.; Galey, J.-B.; Ramos-Stanbury, L.; Taulelle, F.; et al. Impact of Amino Acids on the Isomerization of the Aluminum Tridecamer Al_{13}. *Inorg. Chem.* **2017**, *56*, 12401−12409.
(50) Furrer, G.; Phillips, B. L.; Ulrich, K. U.; Pöthig, R.; Casey, W. H. The Origin of Aluminum Flocs in Polluted Streams. *Science* **2002**, *297*, 2245−2247.
(51) Phillips, B. L.; Ohlin, C. A.; Vaughn, J.; Woerner, W.; Smart, S.; Subramanyam, R.; Pan, L. Solid-State ^{27}Al NMR Spectroscopy of the γ-Al_{13} Keggin Containing Al Coordinated by a Terminal Hydroxyl Ligand. *Inorg. Chem.* **2016**, *55*, 12270−12280.
(52) Haouas, M.; Taulelle, F.; Martineau, C. Recent Advances in Application of 27Al NMR Spectroscopy to Materials Science. *Prog. Nucl. Magn. Reson. Spectrosc.* **2016**, *94*−*95*, 11−36.
(53) Frydman, L. Fundamentals of Multiple-Quantum Magic-Angle Spinning NMR on Half-Integer Quadrupolar Nuclei. *Encyclopedia of Nuclear Magnetic Resonance*; John Wiley & Sons, 2003; Vol. *9*.
(54) Medek, A.; Harwood, J. S.; Frydman, L. Multiple-Quantum Magic-Angle Spinning NMR: A New Method for the Study of Quadrupolar Nuclei in Solids. *J. Am. Chem. Soc.* **1995**, *117*, 12779−12787.
(55) Sipos, P.; Hefter, G.; May, P. M. 27Al NMR and Raman Spectroscopic Studies of Alkaline Aluminate Solutions with Extremely High Caustic Content - Does the Octahedral Species $Al(OH)_6^{3-}$ Exist in Solution? *Talanta* **2006**, *70*, 761−765.
(56) Tossell, J. A. Theoretical Studies on Aluminate and Sodium Aluminate Species in Models for Aqueous Solution: $A1(OH)_3$, $Al(OH)_4^-$, and $NaAl(OH)_4$. *Am. Mineral.* **1999**, *84*, 1641−1649.
(57) Gebauer, D.; Wolf, S. E. Designing Solid Materials from Their Solute State: A Shift in Paradigms toward a Holistic Approach in Functional Materials Chemistry. *J. Am. Chem. Soc.* **2019**, *141*, 4490−4504.
(58) Zhang, Y.; Zheng, S.; Du, H.; Wang, S.; Zhang, Y. Solubility of Al_2O_3 in the Na_2O−Al_2O_3−H_2O−CH_3OH System at (30 and 60) °C. *J. Chem. Eng. Data* **2010**, *55*, 1237−1240.
(59) Stephen, H.; Stephen, T. *Solubilities of Inorganic and Organic Compounds*; Pergamon Press: New York, 1963; Vol *1*.
(60) Graham, D. J.; Midgley, N. G. Graphical Representation of Particle Shape Using Triangular Diagrams: An Excel Spreadsheet Method. *Earth Surf. Processes Landforms* **2000**, *25*, 1473−1477.

https://dx.doi.org/10.1021/acs.jpcc.0c00205
J. Phys. Chem. C 2020, 124, 12337−12345